applied sciences

MDPI

Article

Experimental Study on the Relationship between the Degree of Surrounding Rock Fragmentation and the Adaptability of Anchor Support

Shuai Wang [1], Lianguo Wang [1,*], Furong Tang [2,*], Ke Ding [3], Zhaolin Li [3], Bo Ren [1], Chongyang Jiang [1] and Jiaxing Guo [1]

[1] State Key Laboratory for Geomechanics and Deep Underground Engineering, China University of Mining and Technology, Xuzhou 221116, China; swang@cumt.edu.cn (S.W.); 02140873@cumt.edu.cn (B.R.); chongyang_jiang@cumt.edu.cn (C.J.); guo1jiaxing@126.com (J.G.)

[2] School of Materials Science and Physics, China University of Mining and Technology, Xuzhou 221116, China

[3] State Key Laboratory of Mining Response and Disaster Prevention and Control in Deep Coal Mines, Anhui University of Science and Technology, Huainan 232001, China; dingke@cumt.edu.cn (K.D.); lzhlcumt@163.com (Z.L.)

* Correspondence: cumt_lgwang@163.com (L.W.); tfr96@cumt.edu.cn (F.T.)

Abstract: Taking the roadway peripheral rock anchoring unit as the research object, the rock compression test containing the anchor solid was carried out to analyze the influence of the degree of peripheral rock fragmentation and the anchor support method on the mechanical properties of the rock body. The test results showed that the smaller the size of the structural surface, the more a greater number of anchor rods were needed, which in turn provided better support. With the increase in the size of the structural surface, the uniaxial compressive strength and modulus of elasticity of the specimen showed a gradual decrease. Numerical tests of the uniaxial compression of rock containing cohesive units showed that the deformation of the specimen near the anchor bar was significantly reduced, while the main rupture surface was blocked, and an obvious reinforcement zone was formed near the anchor bar. Under the double-anchor condition, the anchor tension stress was more obvious, the reinforcement zone was wider, and the rock rupture surface was strongly blocked, all of which made its reinforcement effect the more obvious. This double-anchor condition showed that the anchoring effect of the anchor rods on the specimens was reflected in two aspects of reinforcement and crack stopping. The denser the anchor rods, the wider the reinforcement zone and hence the more likely that the superposition effect will occur, which allowed the anchor rods to play a greater supporting role in stabilizing the rock. The research results can provide a theoretical basis for the design of anchor support and early warning prediction of destabilization damage in the fractured surrounding rock of coal mine roadways.

Keywords: anchor support; fractured perimeter rock; similar material simulation; numerical simulation; support mechanism

check for updates

Citation: Wang, S.; Wang, L.; Tang, F.; Ding, K.; Li, Z.; Ren, B.; Jiang, C.; Guo, J. Experimental Study on the Relationship between the Degree of Surrounding Rock Fragmentation and the Adaptability of Anchor Support. *Appl. Sci.* **2023**, *13*, 11328. https://doi.org/10.3390/app132011328

Academic Editor: Syed Minhaj Saleem Kazmi

Received: 26 September 2023
Revised: 10 October 2023
Accepted: 13 October 2023
Published: 15 October 2023

1. Introduction

At this stage, coal is the main energy source in China, with an output of about 4.45 billion tons in 2022, and coal resources account for more than 70% of one-time energy consumption. According to incomplete statistics, more than 90% of China's coal production comes from shaft mining, which requires a large number of roadways to be excavated underground, and it is important to keep the roadways open and the perimeter rock stable for the construction and production of coal mines. The length of newly dug roadways in China is about 12,000 km per year. As a result of the continuous improvement of mining depth, width, and intensity, the depth of the roadway is increasing year by year, and the geological conditions are becoming more and more complicated. Additionally, the complicated and difficult conditions such as high geostress roadways, roadways with strong mining influence, soft and broken perimeter rock roadways, and extra-large section roadways and refuge are becoming more common, which significantly increases the difficulty of the roadway support [1].

As the mining depth increases, the ground stress rises significantly, and the mechanical properties of the deep rock body show different characteristics from those of the shallow rock body [2–6]. Due to the complex geological structure [7], the rock body of underground engineering is usually rich in defects such as joints, faults, and discontinuous surfaces, which can cause different degrees of fragmentation of the surrounding rock and have an important impact on the safe construction of underground engineering and the stability of the surrounding rock [8–11]. Due to the existence of geological structural surfaces in the rock mass, the mechanical strength of the rock mass is greatly reduced, and most engineering practices have proved that the structural surfaces in the rock mass play a controlling role in the deformation and destructive strength of the rock mass. Therefore, an accurate understanding of the deformation and damage law of the rock body containing internal joints is crucial for the reinforcement of weak and broken perimeter rock [12]. Jeon et al. [13] showed that the deformation of the tunnel perimeter rock increased significantly due to the existence of the weak face and obvious shear deformation appearing along the weak face through physical tests and numerical simulation. Meanwhile, Moir et al. [14] illustrated the characteristics of the rock body rupture evolution of the fracture network under the action of the load through numerical calculations and showed that the geometrical distribution of the fracture network was very small. The results of their study showed that the fracture network was not only a good solution, but that it had the effect of the deformation of the rock body as well. The results show that the geometric distribution of the fissure network and the local stress field have an important influence on the development of the rupture zone of the surrounding rock.

In terms of surrounding rock reinforcement technology, anchor support technology, as one of the most common rock reinforcement means, plays an indispensable role in mining engineering, slope reinforcement, and other fields [15,16]. Anchor support significantly improves the tunnel support effect, reduces the cost of tunnel support, and reduces the labor intensity of workers. What is more, anchor support greatly simplifies the end support and overhead support process of the coal mining face, ensures safe production, and creates good conditions for the rapid advancement of the coal mining face and the substantial increase in coal production. At present, anchor support technology has been commonly used at home and abroad and is one of the key technologies essential for coal mines to realize high productivity and high efficiency. It has achieved good results in complex and difficult conditions such as high geostress roadways, soft rock roadways, roadways affected by strong dynamic pressure, and roadways digging and staying along the empty roadways in kilometer-deep wells [17–22]. Its working principle is to fully utilize and improve the bearing capacity of the rock body, which has a good reinforcement effect and economic cost [23–25]. In recent years, many scholars at home and abroad have explored and researched the action mechanism of anchors from various aspects, including some classical theories such as suspension theory, combined beam theory, combined arch theory, perimeter rock loosening circle support theory, and perimeter rock strength reinforcement theory [26,27]. The research methods are mainly divided into indoor tests, model tests, theoretical analysis, and numerical simulation. Li et al. [28] investigated the reinforcing effect of anchors on rock bodies containing penetrating fissures under uniaxial tensile conditions through indoor experiments, and the results showed that the anchored specimens showed plastic damage characteristics and the anchors increased the deformation modulus and uniaxial tensile strength of the jointed rock body. Wong and Chau (1998) and Wong et al. (2001) conducted experiments on rock-like materials containing two and three fissures (rectangular specimen dimensions: $60 \times 120 \times 25$ mm) subjected to uniaxial compression. Their findings revealed that the peak strength of the specimens was not contingent upon the initial crack density but rather on the actual number of pre-existing flaws involved in the coalescence process. Chen et al. [29] carried out tensile-shear tests on the anchored specimens by developing a new test method to characterize the strain distribution of the surface of the anchors under the tensile-shear loading and, at the same time revealed that the angle of the installation of the anchors. In a separate study, Sagong and Bobet [30] examined a series of specimens (rectangular specimen dimensions: 101.6 × 203.2 × 30 mm) composed of gypsum and featuring three and sixteen fissures, which were subjected to uniaxial compression. Their research focused on elucidating the influence of continuity and the ligament influence of continuity and ligament length on the stress associated with crack coalescence. Su et al. [31] simulated the formation process of rock bodies in fault-fracture zones by a novel test method and prefabricated model specimens of anchors anchored by uniaxial. The effect of the anchorage form on the bearing capacity and damage mode of the fault fractured rock body was investigated by compression test. Jing et al. [32] investigated the effect of the nodal angle and anchor density on the anchorage strength, deformation behavior, and axial force evolution characteristics of the anchorage in the model specimen under the action of normal stress by prefabricating a large-scale nodal model specimen (500 mm×500 mm×480 mm). With the continuous development of advanced testing techniques and computer simulation software, unprecedented progress has been made in recent years in the study of anchor support principles. Deb and Das [33] introduced a doubly enriched finite element (DEFE) procedure designed for simulating grouted bolts passing through rock joints. Nie et al. [34] incorporated a rock bolt element, grounded in analytically derived interface behavior, into a two-dimensional discontinuous deformation analysis (DDA) program to assess the effectiveness of the rock reinforcement system, yielding valuable insights into the role of DDA in the design of rock reinforcement systems. Lin et al. [35] constructed a three-dimensional bolt-reinforced model within rock joints using the FLAC3D numerical calculation program. They investigated the influence of bolt inclination angles on both flat and undulating joint surfaces.

In the actual project, due to the influence of primary joints, fissures, and other structural surfaces and weathering and erosion, the surface of the roadways of the soft surrounding rock was highly fragmented, forming irregular bulk block structures of different sizes [36,37]. The surrounding rock had large deformation and strong rheological properties. The bearing capacity and anchoring mechanical behavior of this fractured rock mass were significantly different compared with the intact rock mass [38]. Throughout the literature at home and abroad, experimental studies on the relationship between the degree of surrounding rock fragmentation and the adaptability of anchor support are rarely reported. In view of this, this study, through the development of model-similar materials and a specialized anchor addition scheme, carried out compression tests on the model specimens of similar materials under the action of anchor anchoring to investigate the influence law of aggregate particle size and anchor anchoring method on the strength, deformation, and fracture characteristics of the specimens. And the reinforcing effect of the anchor rods on the soft and broken surrounding rock was analyzed by numerical simulation.

2. Test Program

The traditional combined arch theory believes that if the anchor spacing is relatively close, this double conical compression zone between the anchors overlaps and the combination is arch-shaped, and as a result the extrusion combination action can be formed (see Figure 1). In Figure 1, Region A is one of the anchor units in the combined arch bearing structure, and Region B represents the double-anchor bar anchorage unit. This test is based on the force state of the anchor solid in the surrounding rock. When combined with the effect of the different degrees of fragmentation on the anchoring effect of the anchor rods, the anchor solid can be investigated.

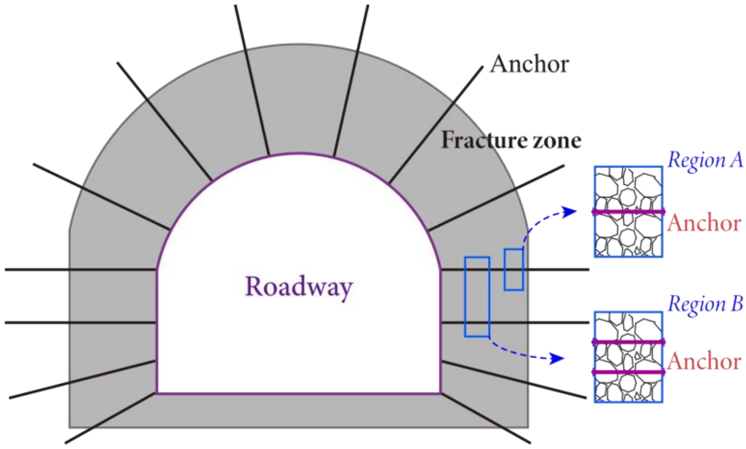

Figure 1. Schematic diagram of the combined arch of the surrounding rocks.

2.1. Modeling

Considering the comparability of the test results, it is recommended to use gypsum and quartz sand as the raw materials to configure the specimens [39]. The specimen size was set to 50 mm × 50 mm × 100 mm with reference to the international standards of rock mechanical testing and the results of previous research [40–43], where gypsum was used as a binder [44]. In order to simulate the large number of fissures and other structural surfaces that exist in the rock mass, three kinds of quartz sand with different grain sizes (Grain size A: 2–4 mm, Grain size B: 4–8 mm, and Grain size C: 10–15 mm) of quartz sand as the aggregate were used (Figure 2). The specimens containing quartz sand and gypsum with different grain sizes were used to simulate rock bodies with different degrees of microfractures and structural surfaces. The smaller grain sizes of quartz sand and gypsum had smaller contact surfaces, forming structural surfaces of smaller sizes inside the specimens, and vice versa.

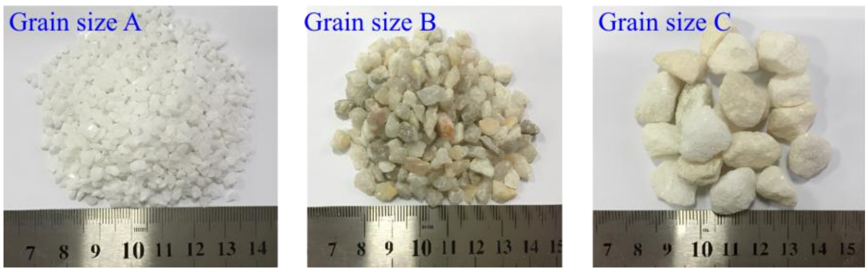

Figure 2. Quartz sand with different grain size.

The steps for preparing the specimens (Figure 3) are as follows:

1. Brush the mold release agent on the inside of 50 mm × 50 mm × 100 mm mold, weigh quartz sand, gypsum, and water separately with a balance and set aside;
2. Put gypsum and quartz sand in a container, add water evenly and mix it quickly, and put it into the mold for vibration (the ratio of materials is water: gypsum: quartz sand = 1:1.5:3);
3. Smooth the upper surface after shaking evenly, and remove the mold 24 h after the specimen is finished;
4. Put the mixture into the drying box at 60 °C for maintenance, after about 10 days of maintenance drying;
5. After the specimen is completely dry, polish the specimen and measure with vernier calipers to ensure that the error is within the allowable range.

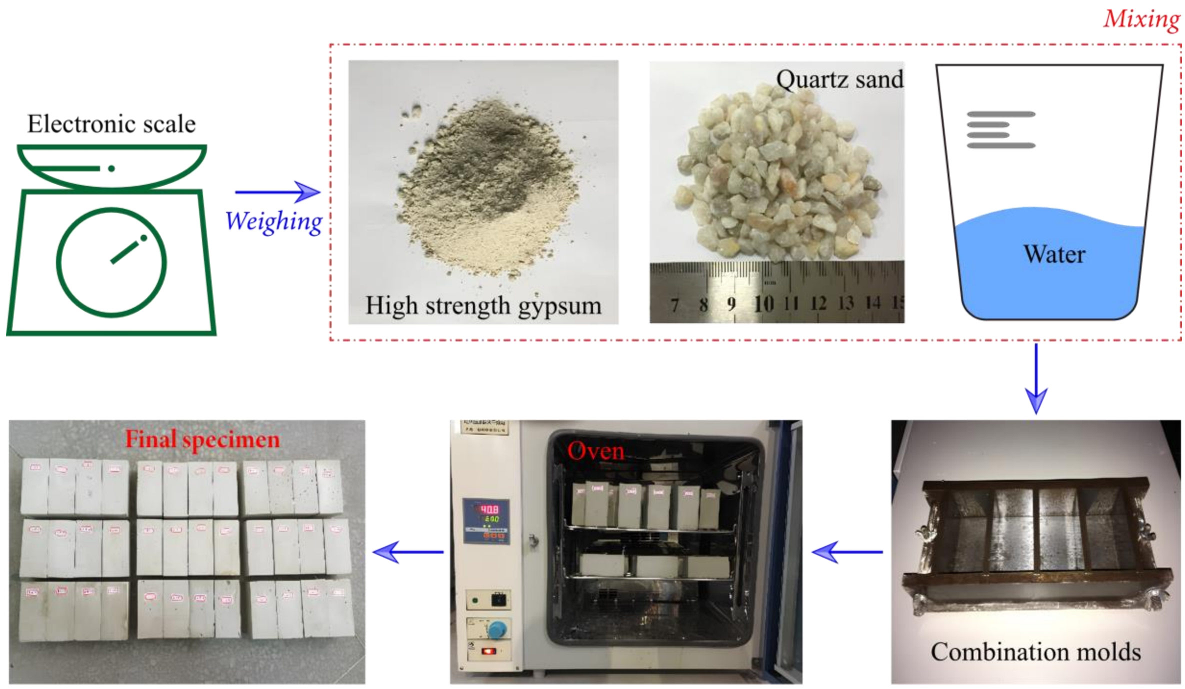

Figure 3. Specimen production process.

After reviewing a large number of studies and the mechanical properties of the materials, based on the similarity theorem, the selection of the anchor rods required that their mechanical properties are basically the same as those used in the project. After comparing the mechanical properties of relevant carbon steel materials, it was decided to select the steel wire processed from No. 45 steel as the anchor rod for this test. The mechanical properties parameters are shown in Table 1.

Table 1. Mechanical Parameters of Common Anchor and Selected Screws.

Materials	Tensile Strength /MPa	Shear Strength /MPa	E/GPa	Anchoring Force /MPa	Elongation/%
General Anchor	200~600	260~600	200	≥50	≥16
Selection of screws	600	400	210	20~40	≥16

The geometric similarity ratio of the anchor parameters selected for this test is 10:1, which can be adjusted according to the actual conditions in the laboratory, and the basic parameters are shown in Table 2.

Table 2. Geometric parameters of specimen anchoring.

Typology	Drilling Diameter /mm	Anchor Diameter /mm	Spacing /mm
Engineering Prototypes	30	20	800
Anchoring specimen	3	2	80

Drill anchor holes in the horizontal direction of the test piece using a bench drill. Screw the nut and spacer on one end of the anchor rod and insert it into the drilled anchor hole on the test piece. Add the spacer on the other end and tighten it with the nut while applying a certain amount of preload.

It was decided to select the double-ended steel wire screw processed from No. 45 steel as the reinforcing anchor rod for this test with the use of fastening nuts and circular spacers.

The tensile strength of the anchor was 600 MPa, the modulus of elasticity was 210 GPa, and the elongation was ≥16%. The holes were drilled horizontally in the specimen with a diameter of 2 mm using a bench drill, one end of the anchor rod was screwed with a nut and a spacer and inserted into the drilled holes in the specimen, and the spacer was added and fastened with a nut on the other side, while applying a certain amount of pre-tensioning force. The specimens made of each grain size aggregate were arranged with 0, 1, and 2 anchors, respectively, and the finished fabricated plus anchor body is shown in Figure 4.

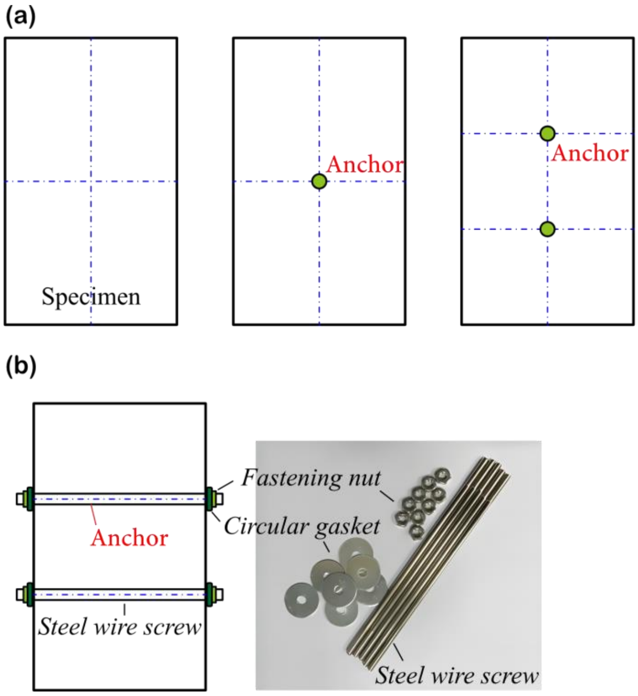

Figure 4. (**a**) Anchoring specimen layout; (**b**) Anchoring specimen.

2.2. Test Methods

A RLJW-2000 microcomputer-controlled rheological experimental machine was used to carry out the rock unidirectional compression test, as shown in Figure 5. The data of the stress can be measured by the experimental machine by placing two micrometers at the diagonal of the chassis for measuring the axial deformation of the specimen. This test was loaded at the rate of 0.25 mm/min until the specimen completely loses the load-bearing capacity, and the results of the experiment were compared to analyze the effect of the anchor on the uniaxial compressive strength of the specimens of different types and the damage characteristics of the experimental program, as shown in Table 3.

Table 3. Test program.

Group/Type of Specimen	Anchor Type	Specimen Number
Grain size A: 2–4 mm aggregate	0 anchor 1 anchor 2 anchors	1-0-1~1-0-4 1-1-1~1-1-4 1-2-1~1-2-4
Grain size B: 4–8 mmaggregate	0 anchor 1 anchor 2 anchors	2-0-1~2-0-4 2-1-1~2-1-4 2-2-1~2-2-4
Grain size B: 10–15 mmaggregate	0 anchor 1 anchor 2 anchors	3-0-1~3-0-4 3-1-1~3-1-4 3-2-1~3-2-4

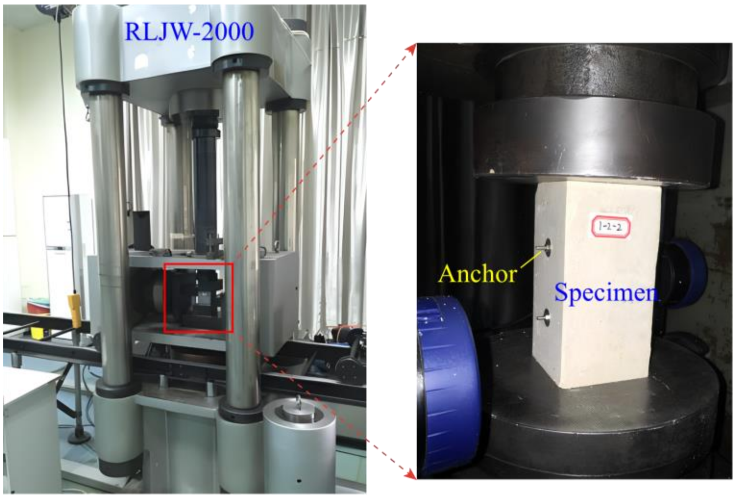

Figure 5. Test setup and specimen loading.

3. Results

3.1. Stress–Strain Curve of Anchor Solid

The axial stress–strain curves during uniaxial compression of the specimens with different grain sizes are shown in Figure 6. Compared with the unanchored specimen, it can be seen that the residual strength value of the anchored specimen in the late stage of damage had a greater increase, but the residual strength value in the compression process of the 2–4 mm grain size aggregate specimen was higher than that of the 4–8 mm and 10–15 mm grain size aggregate specimens. Consequently, the trend of the stress–strain curves of the larger aggregate specimens close to the horizontal direction was more obvious. This indicates that under uniaxial compression conditions, anchors can increase the compressive strength and elastic modulus of specimens. They can also improve the residual strength of the rock mass, but the ability of the anchor bar to improve the residual strength of the rock mass gradually decreases with the increase in the specimen crushing degree.

Comparing the stress–strain curves of the different types of anchored specimens and unanchored specimens revealed that the anchors change the deformation characteristics of the surrounding rock body. Under the no-anchor condition, the brittle characteristics of the rock-like body specimens were more obvious, and when the specimen reached the peak strength, i.e., when the specimen reached the limit of its ability to resist the external load, the rate of decrease in the stress–strain postpeak curves was faster, and the postpeak modulus was larger. For the anchored specimen, its brittle characteristics were not obvious, and the deformation of the anchored rock body showed plastic characteristics. When the anchored rock sample reached the peak compressive strength, the peak stress–strain curve began to decline. Compared to the unanchored specimen, the stress decline rate was reduced, and when the stress dropped to a certain value, the stress–strain curve of the specimen had a small fluctuation, that is, the specimen stress decline rate was small with regard to the anchor at this time. The role of the anchor was more obvious. There was no-anchor specimen in the load loading process. When the specimen reached the peak compressive strength, the rate of stress decline was faster. When the anchor specimen reached the peak strength in the rupture process, the anchor bar prevented internal cracks from expanding and penetrating inside the specimen, thus slowing down the rupture rate.

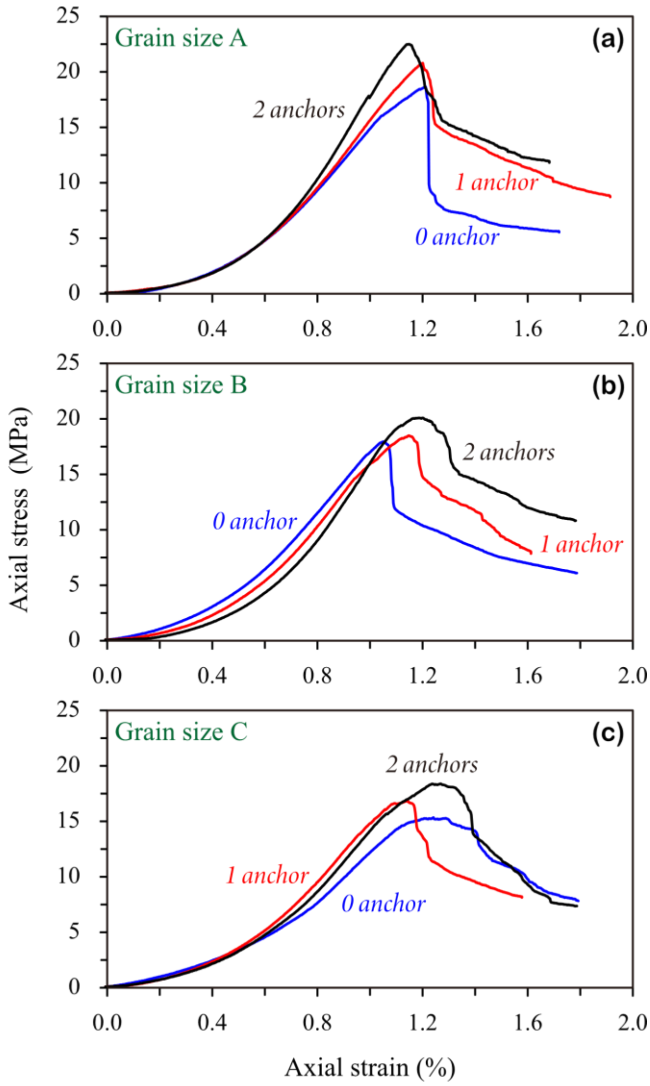

Figure 6. Stress–strain curve of anchor solid. (**a**–**c**) represent anchor solids composed of particle sizes of 2–4 mm, 4–8 mm, and 10–15 mm, respectively.

The uniaxial compressive strength of the specimens with quartz sand of different grain sizes as the aggregate showed significant differences. These specimens had a smaller surface area for the smaller grain size quartz sand aggregate, a smaller contact surface for gypsum, and the formation of structural surfaces of smaller sizes inside the specimen with a smaller degree of fragmentation, while they also had a larger surface area for the larger grain size quartz sand aggregate, a larger contact surface for gypsum, and the formation of structural surfaces of larger sizes inside the specimen with a higher degree of fragmentation. The change characteristics of the compressive strength and elastic modulus of the rock mass under the conditions of the different grain sizes and anchoring methods are shown in Figure 7. It is worth explaining that the modulus of elasticity of the rock mass in the test is the slope of the approximate straight line segment of the axial stress–strain curve, i.e., the generalized modulus of elasticity, as can be seen from the diagram:

1. The uniaxial compressive strength and modulus of elasticity of the specimens showed the following pattern: small-size aggregate specimen > medium-size aggregate specimen > large-size aggregate specimen. The average compressive strength of the unanchored specimens with 2–4 mm aggregate (Grain size A) was 19.75 MPa, that of the unanchored specimens with 4–8 mm aggregate (Grain size B) was 18.30 MPa, and that of the unanchored specimens with 10–15 mm aggregate (Grain size C) was

16.94 MPa. Uniaxial compressive strength decreased by 7.34% and 14.23%, respectively. The average modulus of elasticity of the unanchored specimens with 2–4 mm aggregate was 3.074 GPa, the average modulus of elasticity of the unanchored specimens with 4–8 mm aggregate was 2.884 GPa, and that of the unanchored specimens with 10–15 mm aggregate was 2.549 GPa, with the modulus of elasticity decreasing by 6.18% and 17.06%, respectively.

2. The anchoring effect of the anchors on the specimens of different grain sizes varied. For the specimens with different grain sizes of the aggregates with the different anchoring methods, the uniaxial compressive strength and elastic modulus of the specimens followed this pattern: no anchor < single anchor < double anchor. Among them, the uniaxial compressive strength of the specimens with 2–4 mm aggregate size increased by 12.90% and 22.81%, and the modulus of elasticity increased by 16.39% and 23.34%, respectively, compared with that without the anchor in the single-anchored and double-anchored specimens; the uniaxial compressive strength of the specimens with 4–8 mm aggregate size increased by 4.16% and 11.35%, and the modulus of elasticity increased by 3.33% and 14.34%, respectively, compared with that without the anchor in the single-anchored and double-anchored specimens, which increased by 3.33% and 14.25%; the specimens with 10–15 mm particle size aggregate increased the uniaxial compressive strength by 4.88% and 6.02% and the modulus of elasticity by 7.19% and 9.16%, respectively, when the single and double anchored were compared to the unanchored.
3. With the increase in the specimen aggregate particle size, the degree of improvement of the mechanical properties of the anchor rods on the specimen gradually decreased, due to the formation of large-size aggregate and the gypsum size of the structural surface. Because the specimen crushing degree was larger, the anchoring effect of the anchor rods could not be given full play in the crushed rock, and the anchor rods on the crushed rock support adaptability was reduced. Therefore, under the condition of roadways surrounded by rock with a high degree of crushing, auxiliary support measures need to be taken to form a joint coordinated support form to control the phenomenon of a poor anchor support effect of the crushed surrounding rock, the large deformation of roadways surrounded by rock, and other phenomena affecting the safe production of the mine.

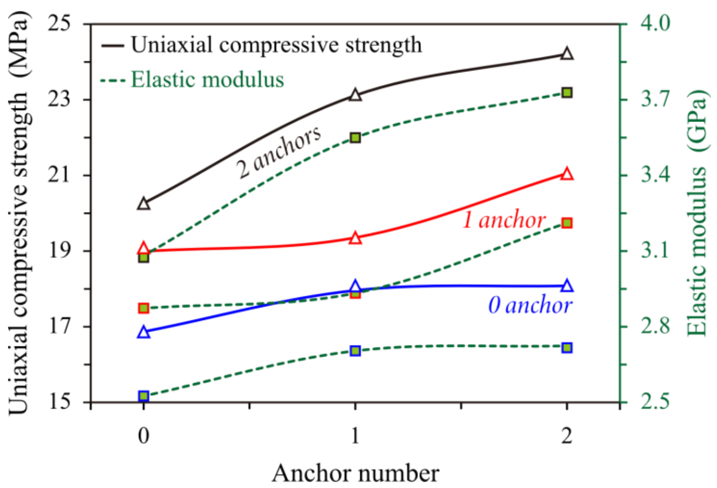

Figure 7. Influence of the degree of surrounding rock fragmentation and the number of anchors added on the mechanical parameters of the rock mass.

3.2. Rupture Characteristics

The final damage pattern of the rock mass under the conditions of different grain sizes and anchoring methods is shown in Figure 8. As can be seen from the graph,

1. Under the condition of no anchor (0 anchor), the uniaxial compression of the specimen formulated with large-grained aggregate was more serious than that of the small-grained aggregate specimen. The specimen as a whole showed diagonal shear damage, but the secondary fissures showing splitting damage developed to a high degree, and different sizes of block spalling phenomenon appeared. When the aggregate diameter was 2–4 mm (Grain size A), the specimen split along the axial direction, i.e., the morphology of the rupture surface was parallel to the loading axial direction, and no shear rupture occurred; when the aggregate diameter was 4–8 mm (Grain size B), the shear rupture was relatively slight, and the shear rupture surface was not completely through the upper and lower parts of the rupture surface; and when the aggregate diameter was 10–15 mm (Grain size C), obvious shear damage occurred on the free surface, and a large number of block spalling phenomenon occurred. This shows the strength difference of the specimens made of the aggregates with different grain size ratios.
2. Under the action of the single anchor (1 anchor), the rock body along the anchor direction was subjected to a certain support resistance constraint, and the rupture of the specimen was relatively homogenized. The rupture crack direction of the rock body changed, the main rupture cracks in the aggregate diameter of 2–4 mm and 4–8 mm rupture cracks in the anchor position rupture crack direction changed at a certain angle, compared with the no-anchor condition rupture degree, which was small; 10–15 mm aggregate single-anchor specimens produced intensive rupture cracks, appearing to a certain extent of the block exfoliation. Combined with the rupture surface of the specimen under the anchored condition in Figure 8, the anchoring effect of the anchor on the specimen was reflected in the two aspects of reinforcement and crack stopping. Under the pre-stressing effect of the anchor, when the crack developed to the range of the anchor's action, the anchor played the role of stopping the crack from developing or changing the direction. The role of the tray along the anchor axial force was applied, and when the tray was in contact with the formation of conical stress concentration within the rock mass, the rock mass played a reinforcing effect.
3. Under the double-anchor condition (2 anchors), the damage pattern of the anchored rock body, when compared with single anchor with an aggregate diameter of 2–4 mm, had less developed specimen secondary cracks; when the aggregate diameter was 4–8 mm, the main rupture cracks were distributed along the direction of the axial stress, and the specimen underwent splitting damage, and the secondary cracks were obviously reduced. When the aggregate diameter was 10–15 mm, the rupture cracks produced by the single-anchor specimen are greater. When the aggregate diameter was 10–15 mm, the rupture cracks produced by the single-anchor specimens were intensive, and those produced by the double-anchor specimens were relatively scattered. This shows that the increase in anchors effectively enhanced the cementation between the anchors and the rock body, which can augment the supporting role of anchors, thus alleviating the degree of rupture of the rock body and improving the overall bearing capacity.

The anchoring effect of the anchor on the specimen was reflected in the two aspects of reinforcement and crack stopping. Under the prestressing reinforcement of the anchor, when the crack developed into the reinforcement range of the anchor, the anchor played the role of stopping the crack from developing or changing its direction. The action of the tray exerting force along the axial direction of the anchor rods created a conical stress concentration within the rock mass in contact with the tray, which acted as a reinforcement to the rock mass. As shown in Figure 9, after the rupture of the specimen, an obvious reinforcement zone was formed at the anchor reinforcement, and this extrusion reinforcement effect improved the integrity and bearing capacity of the rock mass.

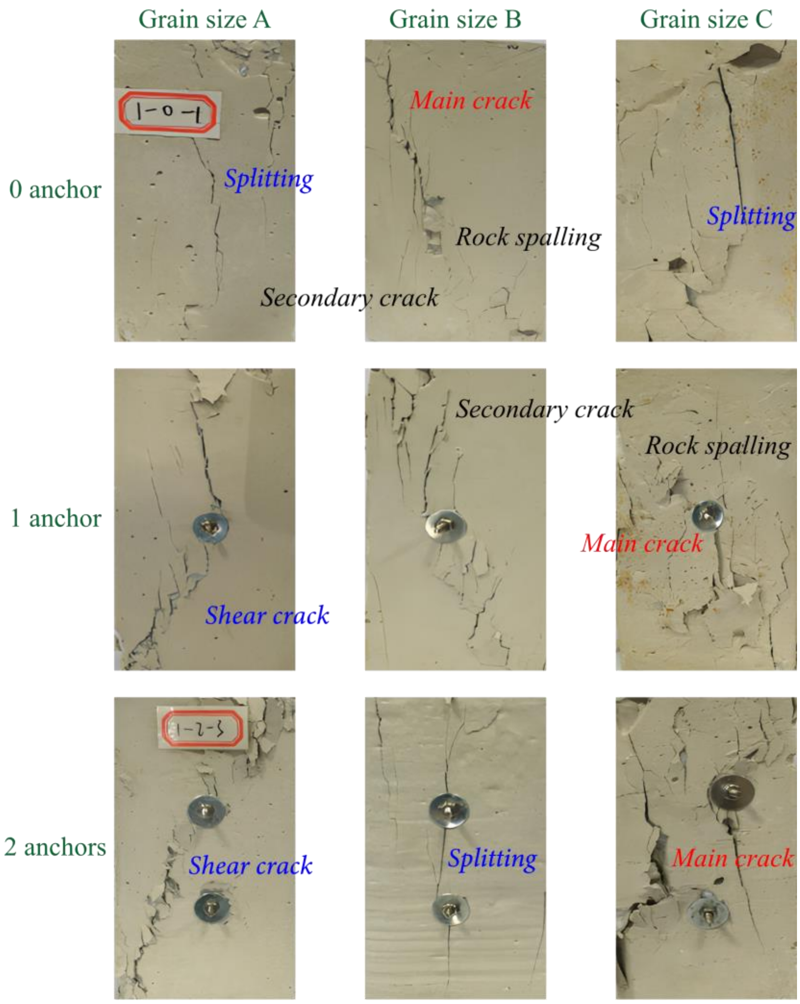

Figure 8. Rupture morphology of specimens with different grain sizes.

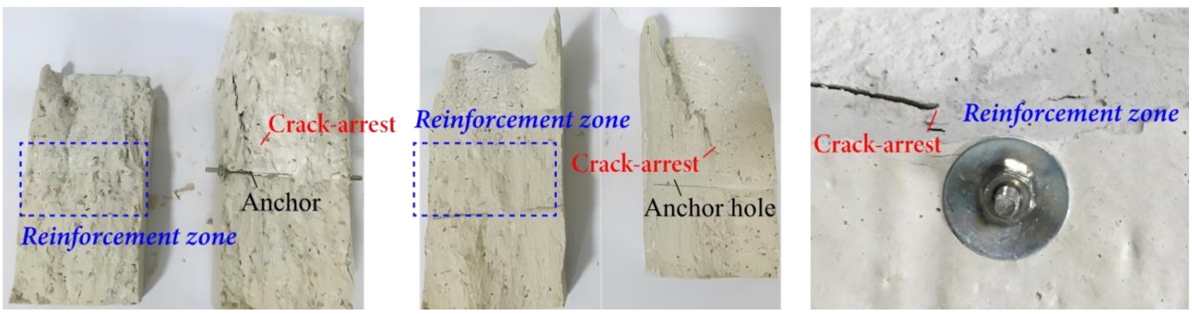

Figure 9. Anchor solid specimen rupture pattern.

4. Numerical Modeling

In order to further analyze the protective effect of the anchor rods on the rock, this paper used the finite element software ABAQUS [45–47] to establish a numerical model of uniaxial compression of the rock. The boundary conditions of the model were similar to the boundary conditions of the test, and the bottom boundary of the model was fixed to the vertical displacement, and the top boundary gradually applied the axial load. The test was divided into three cases: (1) no anchor; (2) embedded 1 anchor; (3) embedded 2 anchors (Figure 10). In the model, cohesive units were inserted between the rock units based on the damage mechanics theory. The rock matrix material parameters were a modulus of elasticity of 10 GPa, a Poisson's ratio of 0.25, and a density of 1700 kg/m^3. The cohesive unit adopted the traction-separation theorem, the fracture energy of the unit was 0.1 N/mm, and it was assumed that there is no friction on the contact surface once the unit is cracked. The anchor material parameters were a modulus of elasticity of 210 GPa and a Poisson's ratio of 0.3.

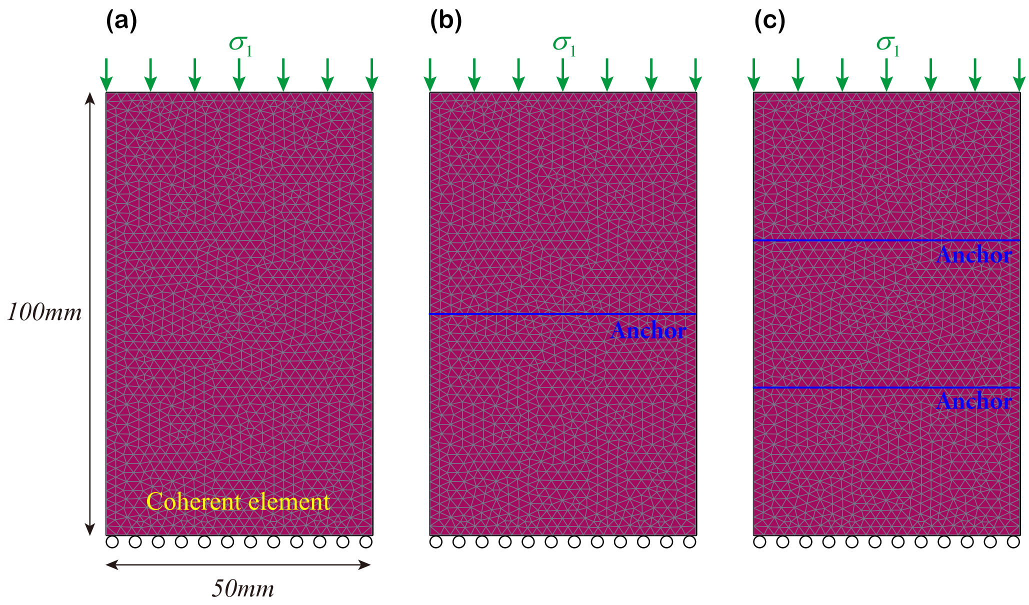

Figure 10. Numerical model of anchor solid. (**a**–**c**) denote the anchored solid consisting of no anchor specimen, 1 anchor specimen, and 2 anchor specimens, respectively.

5. Discussion of the Results

Figure 11 shows the evolution of rock deformation and damage under the different working conditions. For the no-anchor condition (0 anchor), the specimen showed typical oblique shear damage characteristics, and at the same time, in the region near the top and bottom boundaries, a block spalling phenomenon occurred, and with the continuous increase in the axial load, the main macroscopic rupture surface running through the specimen was presented eventually. Under the single-anchor action (1 anchor), the deformation of the specimen near the anchor was significantly lower than that in other areas due to the limiting effect of the anchor. At the same time, the main rupture surface of the rock was blocked, and it can be seen from the figure that an obvious reinforcement zone was formed near the anchor. Under the condition of double anchors (2 anchors), the restriction effect of anchors was more obvious, the range of strengthened area was wider, and the rock rupture surface was strongly blocked. This indicates that the anchors played a reinforcing and fracture stopping role on the rock, and the more anchors (or the more intensive) meant a more obvious reinforcing effect.

Figure 12 shows the maximum stress distribution characteristics of the anchor solid. From the figure, it can be seen that due to the embedded anchor in the specimen, the lateral expansion of the specimen occurred after the external load was applied, and the tensioning effect of the anchor was obvious. The specimen gradually produced oblique shear damage near the top-bottom boundary. However, due to the tensile action of the anchor rods, the crack expansion was inhibited, and the tension stress of the anchor rods near the potential rupture area (ellipse area) in the figure was more obvious (the anchor rods are in the red color, which represents a higher stress), which indicates that the anchor rods played a role of reinforcing and stopping cracks in the rock, and the more densely the anchors were installed, the more obvious their reinforcing effect was.

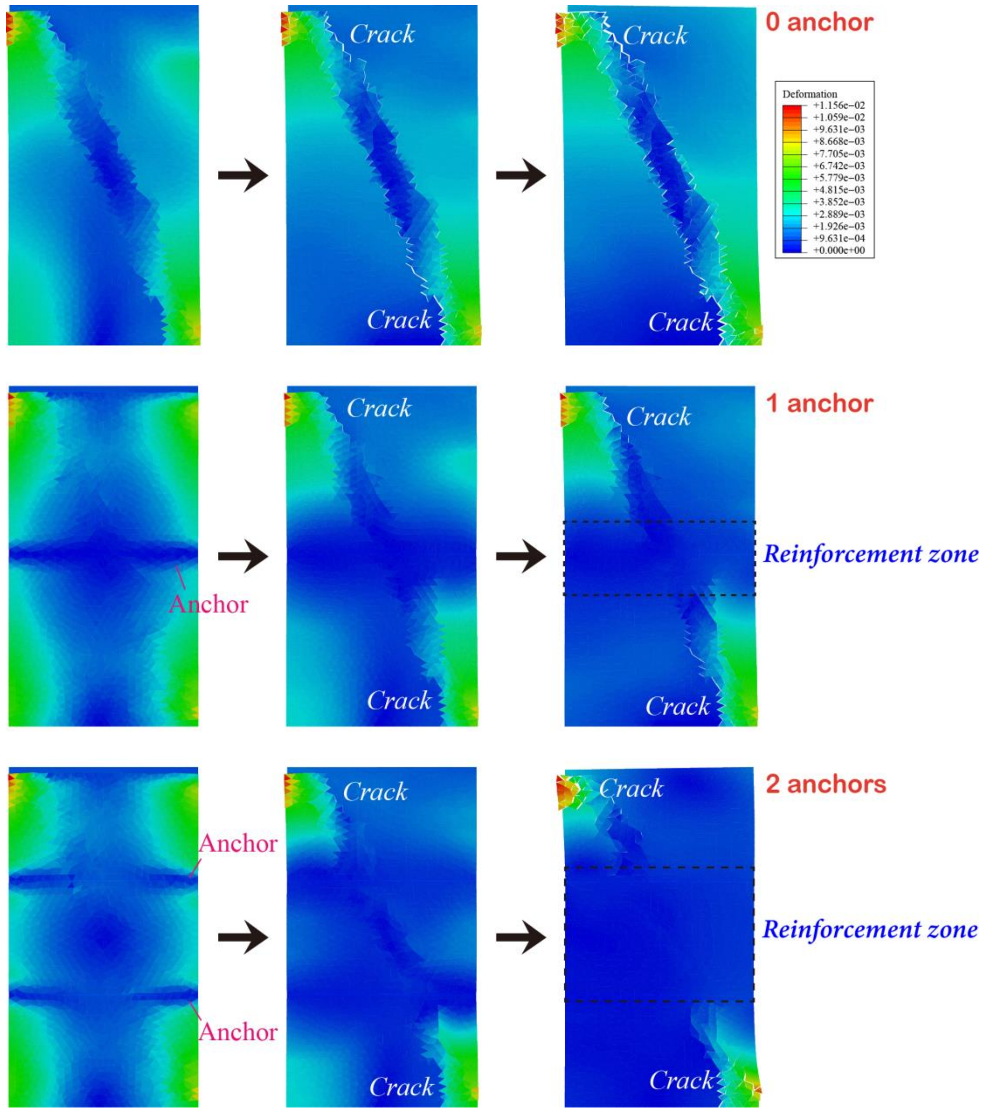

Figure 11. Deformation damage cloud diagram of different specimens.

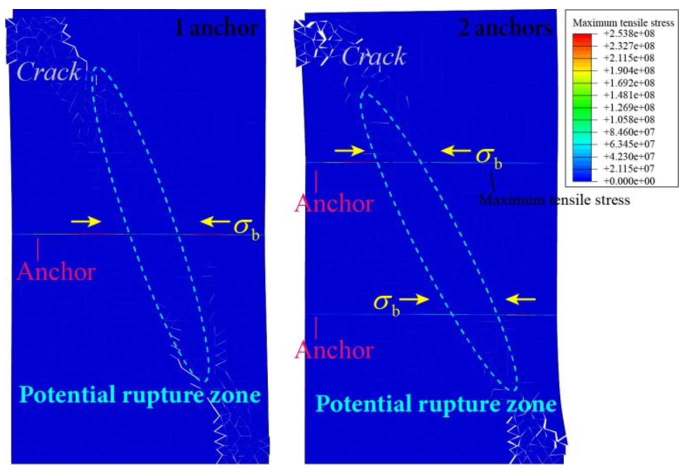

Figure 12. Characterization of the maximum stress distribution in the anchor solid.

Figure 13 shows a schematic diagram of the reinforcing action of the anchor rods, from which it can be seen that the anchor rods limited the deformation of the specimen and formed an anchor support anchorage force, similar to a small lateral circumferential pressure. In the area of anchor cementation and action, a reinforcement zone was formed, which can greatly limit the development of internal cracks as well as the lateral expansion of the rock and provide protection to the specimen. Compared with the limited scope of the reinforced zone under the single-anchor condition, the reinforced zone under the double-anchor condition had a wider scope, and there was a superposition effect, which effectively strengthened the bonding effect of the anchor and the rock body. This, as a result, gave a better supporting effect to the anchor, which greatly alleviated the rock's rupture development, effectively harmonized its overall deformation, and played a key role in stabilizing it.

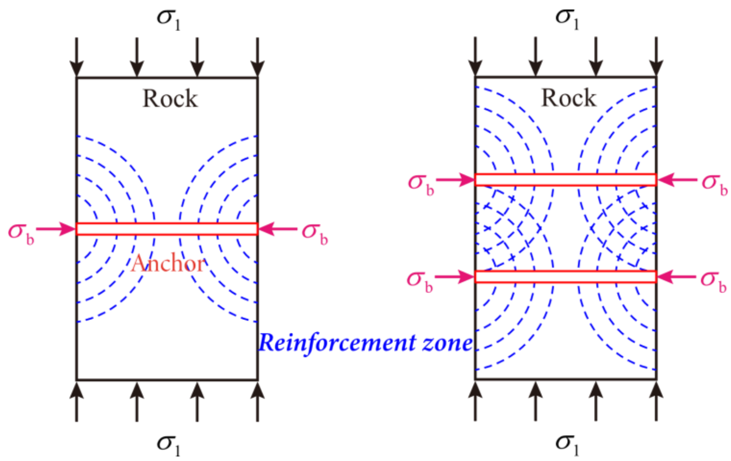

Figure 13. Schematic diagram of the reinforcing effect of anchors. Σ_b represents maximum tensile stress.

6. Conclusions

1. The uniaxial compressive strength of the specimens with different grain size quartz sand as the aggregate showed significant differences, with a smaller surface area for the smaller grain size quartz sand aggregate, a smaller contact surface for gypsum, which formed smaller size structural surfaces inside the specimen and had a smaller degree of fragmentation, whereas the larger grain size quartz sand aggregate formed larger size structural surfaces inside the specimen and a higher degree of fragmentation. The uniaxial compressive strength and modulus of elasticity of the specimens showed the following pattern: small-size aggregate specimen > medium-size aggregate specimen > large-size aggregate specimen.
2. Compared with the specimen without the anchor, the residual strength value of the anchored specimen in the late stage of damage had a greater increase, but the residual strength value was higher than that of the large aggregate specimen in the compression process of the small aggregate specimen, and the trend of the stress–strain curve close to the horizontal direction was more obvious in the specimen of the larger aggregate size. This shows that under uniaxial compression, the anchor can not only improve the compressive strength and elastic modulus of the rock mass but it can also improve the residual strength of the rock mass. However, with the increase in specimen crushing degree, the ability of the anchor to improve the residual strength of the rock mass gradually decreased.
3. The anchoring effect of the anchors on the specimens with different grain sizes varies was crucial. When different anchoring methods are used for the specimens with the different grain sizes of the aggregates, the uniaxial compressive strength and elastic modulus of the specimens follow the following pattern: no anchor<single anchor<double anchor. With the increase in the specimen aggregate size, the degree of improvement of the mechanical properties of the specimens by the anchors decreases gradually.

4. Numerical tests on the uniaxial compression of the rock containing cohesive units were carried out. It was found that under the no-anchor condition, the specimen showed typical oblique shear damage characteristics, and under the single-anchor action, the deformation of the specimen near the anchor bar was obviously reduced. By contrast, the main rupture surface was blocked, and an obvious reinforcement zone was formed near the anchor bar. Under the double-anchor condition, the anchor tension stress was more obvious, the reinforcement zone was wider, and the rock rupture surface was strongly blocked, all of which made its reinforcement effect the more obvious.
5. The anchoring effect of the anchor on the specimen was reflected in the two aspects of reinforcement and crack stopping. Under the prestressing effect of the anchor, when the crack developed to the range of the anchor's action, the anchor played the role of stopping the crack from developing or changing its direction. After the specimen rupture, an obvious conical reinforcement zone was formed at the anchor reinforcement, and this extrusion reinforcement effect improved the integrity and bearing capacity of the rock mass. Moreover, the denser the anchors, the wider the reinforcement zone, and the superposition effect occurred, which better utilized the supporting role of the anchors and played a key role in stabilizing the rock.

Author Contributions: Conceptualization, L.W.; methodology, Z.L.; software, Z.L. and C.J.; validation, B.R.; formal analysis, B.R. and S.W.; investigation, S.W., K.D. and J.G.; resources, F.T.; data curation, S.W. and K.D.; writing—original draft preparation, S.W.; writing—review and editing, S.W.; visualization, C.J.; supervision, F.T. and J.G.; project administration, F.T.; funding acquisition, L.W. All authors have read and agreed to the published version of the manuscript.

Funding: This work was supported by the National Key Research and Development Program of China (No. 2017YFC0603004), Scientific Research Foundation for High-level Talents of Anhui University of Science and Technology (No. 2022yjrc37) and Open Research Foundation for State Key Laboratory of Mining Response and Disaster Prevention and Control in Deep Coal Mines (No. SKLMRDPC22KF05).

Institutional Review Board Statement: Not applicable.

Informed Consent Statement: Not applicable.

Data Availability Statement: Not applicable.

Conflicts of Interest: The authors declare no conflict of interest.

References

1. Kang, H. Support technologies for deep and complex roadways in underground coal mines: A review. *Int. J. Coal Sci. Technol.* **2014**, *1*, 261–277. [CrossRef]
2. He, M.C. Rock mechanics and hazard control in deep mining engineering in China. *Rock Mech. Undergr. Constr.* **2006**. [CrossRef]
3. Sun, J.; Wang, S. Rock mechanics and rock engineering in China: Developments and current state-of-the-art. *Int. J. Rock Mech. Min. Sci.* **2000**, *37*, 447–465. [CrossRef]
4. Xie, H.; Lu, J.; Li, C.; Li, M.; Gao, M. Experimental study on the mechanical and failure behaviors of deep rock subjected to true triaxial stress: A review. *Int. J. Min. Sci. Technol.* **2022**, *32*, 915–950. [CrossRef]
5. Xie, H.; Gao, F.; Ju, Y. Research and development of rock mechanics in deep ground engineering. *Chin. J. Rock Mech. Eng.* **2015**, *34*, 2161–2177.
6. Chai, Y.; Dou, L.; Cai, W.; Małkowski, P.; Li, X.; Gong, S.; Bai, J.; Cao, J. Experimental investigation into damage and failure process of coal-rock composite structures with different roof lithologies under mining-induced stress loading. *Int. J. Rock Mech. Min. Sci.* **2023**, *170*, 105479. [CrossRef]
7. Yoon, S.; Lee, H.; Kim, J. The modeling of fault activation, slip, and induced seismicity for geological CO_2 storage at a pilot-scale site in the Janggi Basin, South Korea. *Int. J. Rock Mech. Min. Sci.* **2023**, *170*, 105441. [CrossRef]
8. Ju, Y.; Zhang, Q.; Yang, Y.; Xie, H.; Gao, F.; Wang, H. An experimental investigation on the mechanism of fluid flow through single rough fracture of rock. *Sci. China Technol. Sci.* **2013**, *56*, 2070–2080. [CrossRef]
9. Yin, Q.; Jing, H.; Zhu, T. Mechanical behavior and failure analysis of granite specimens containing two orthogonal fissures under uniaxial compression. *Arab. J. Geosci.* **2015**, *9*, 31. [CrossRef]

10. Lee, H.; Jeon, S. An experimental and numerical study of fracture coalescence in pre-cracked specimens under uniaxial compression. *Int. J. Solids Struct.* **2011**, *48*, 979–999. [CrossRef]
11. Zhang, B.; Li, S.; Yang, X.; Zhang, D.; Shao, C.; Yang, W. Uniaxial compression tests on mechanical properties of rock mass similar material with cross-cracks. *Rock Soil Mech.* **2012**, *33*, 3674–3679.
12. Wu, W.; Gong, F.; Ren, L.; He, L. Strain rockburst failure characteristics and mechanism of high stress circular hard rock tunnel triggered by dynamic impact load. *Int. J. Rock Mech. Min. Sci.* **2023**, *171*, 105575. [CrossRef]
13. Jeon, S.; Kim, J.; Seo, Y.; Hong, C. Effect of a fault and weak plane on the stability of a tunnel in rock—A scaled model test and numerical analysis. *Int. J. Rock Mech. Min. Sci.* **2004**, *41*, 658–663. [CrossRef]
14. Moir, H.; Lunn, R.J.; Shipton, Z.K.; Kirkpatrick, J.D. Simulating brittle fault evolution from networks of pre-existing joints within crystalline rock. *J. Struct. Geol.* **2010**, *32*, 1742–1753. [CrossRef]
15. Wang, J.; Apel, D.B.; Xu, H.; Wei, C.; Skrzypkowski, K. Evaluation of the Effects of Yielding Rockbolts on Controlling Self-Initiated Strainbursts: A Numerical Study. *Energies* **2022**, *15*, 2574. [CrossRef]
16. Wang, Q.R.; Xie, L.X.; Song, E.X.; Kong, F.L.; Fan, J.Q.; Yu, L.Y.; Xu, J.M.; Shi, X.Y. Model tests on dynamic responses of surrounding rock and support structure on underground tunnel under combined dynamic and static loading. *Int. J. Rock Mech. Min. Sci.* **2023**, *171*, 105572. [CrossRef]
17. Li, C.C.; Stjern, G.; Myrvang, A. A review on the performance of conventional and energy-absorbing rockbolts. *J. Rock Mech. Geotech. Eng.* **2014**, *6*, 315–327. [CrossRef]
18. Kang, H.; Wu, Y.; Gao, F.; Jiang, P.; Cheng, P.; Meng, X.; Li, Z. Mechanical performances and stress states of rock bolts under varying loading conditions. *Tunn. Undergr. Space Technol.* **2016**, *52*, 138–146. [CrossRef]
19. Huang, Z.; Broch, E.; Lu, M. Cavern roof stability—Mechanism of arching and stabilization by rockbolting. *Tunn. Undergr. Space Technol.* **2002**, *17*, 249–261. [CrossRef]
20. Skrzypkowski, K.; Korzeniowski, W.; Zagórski, K.; Dudek, P. Application of Long Expansion Rock Bolt Support in the Underground Mines of Legnica–Głogów Copper District. *Stud. Geotech. Et Mech.* **2017**, *39*, 47–57. [CrossRef]
21. Cao, R.; Cao, P.; Lin, H. Support technology of deep roadway under high stress and its application. *Int. J. Min. Sci. Technol.* **2016**, *26*, 787–793. [CrossRef]
22. Chen, Y.; Meng, Q.; Xu, G.; Wu, H.; Zhang, G. Bolt-grouting combined support technology in deep soft rock roadway. *Int. J. Min. Sci. Technol.* **2016**, *26*, 777–785. [CrossRef]
23. Chen, S.H.; Yang, Z.M.; Wang, W.M.; Shahrour, I. Study on Rock Bolt Reinforcement for a Gravity Dam Foundation. *Rock Mech. Rock Eng.* **2012**, *45*, 75–87. [CrossRef]
24. Wang, J.; Li, S.-C.; Li, L.-P.; Zhu, W.; Zhang, Q.-Q.; Song, S.-G. Study on anchorage effect on fractured rock. *Steel Compos. Struct.* **2014**, *17*, 791–801. [CrossRef]
25. Zhang, B.; Li, S.; Xia, K.; Yang, X.; Zhang, D.; Wang, S.; Zhu, J. Reinforcement of rock mass with cross-flaws using rock bolt. *Tunn. Undergr. Space Technol.* **2016**, *51*, 346–353. [CrossRef]
26. Wang, J. New development of rock bolting technology for coal roadway in China. *J. China Coal Soc.* **2007**, *32*, 113–118.
27. Liu, Q.; Lei, G.; Peng, X. Advance and review on the anchoring mechanism in deep fractured rock mass. *Chin. J. Rock Mech. Eng.* **2016**, *35*, 312–332.
28. Li, S.; Zhang, N.; Lu, A.; Li, M.; Yang, L. Experimental study of anchoring effect of discontinuous jointed rock mass under uniaxial tension. *Chin. J. Rock Mech. Eng.* **2011**, *30*, 1579–1586.
29. Chen, Y. Experimental study and stress analysis of rock bolt anchorage performance. *J. Rock Mech. Geotech. Eng.* **2014**, *6*, 428–437. [CrossRef]
30. Sagong, M.; Bobet, A. Coalescence of multiple flaws in a rock-model material in uniaxial compression. *Int. J. Rock Mech. Min. Sci.* **2002**, *39*, 229–241. [CrossRef]
31. Su, H.; Jing, H.; Zhao, H.; Yu, L.; Wang, Y. Strength degradation and anchoring behavior of rock mass in the fault fracture zone. *Environ. Earth Sci.* **2017**, *76*, 179. [CrossRef]
32. Jing, H.W.; Yang, S.Q.; Zhang, M.L.; Xu, G.A.; Chen, K.F. An experimental study on anchorage strength and deformation behavior of large-scale jointed rock mass. *Tunn. Undergr. Space Technol.* **2014**, *43*, 184–197. [CrossRef]
33. Deb, D.; Das, K.C. A new doubly enriched finite element for modelling grouted bolt crossed by rock joint. *Int. J. Rock Mech. Min. Sci.* **2014**, *70*, 47–58. [CrossRef]
34. Nie, W.; Zhao, Z.; Ning, Y.; Sun, J. Development of rock bolt elements in two-dimensional discontinuous deformation analysis. *Rock Mech. Rock Eng.* **2014**, *47*, 2157–2170. [CrossRef]
35. Lin, H.; Xiong, Z.; Liu, T.; Cao, R.; Cao, P. Numerical simulations of the effect of bolt inclination on the shear strength of rock joints. *Int. J. Rock Mech. Min. Sci.* **2014**, *66*, 49–56. [CrossRef]
36. Grasselli, G. Manuel Rocha Medal Recipient Shear Strength of Rock Joints Based on Quantified Surface Description. *Rock Mech. Rock Eng.* **2006**, *39*, 295. [CrossRef]
37. Lee, J.S.; Bang, C.S.; Mok, Y.J.; Joh, S.H. Numerical and experimental analysis of penetration grouting in jointed rock masses. *Int. J. Rock Mech. Min. Sci.* **2000**, *37*, 1027–1037. [CrossRef]
38. Fan, L.; Liu, S. A conceptual model to characterize and model compaction behavior and permeability evolution of broken rock mass in coal mine gobs. *Int. J. Coal Geol.* **2017**, *172*, 60–70. [CrossRef]

39. Li, S.C.; Wang, Q.; Wang, H.T.; Jiang, B.; Wang, D.C.; Zhang, B.; Li, Y.; Ruan, G.Q. Model test study on surrounding rock deformation and failure mechanisms of deep roadways with thick top coal. *Tunn. Undergr. Space Technol.* **2015**, *47*, 52–63. [CrossRef]
40. Brown, E.T. (Ed.) *Rock Characterization, Testing & Monitoring: ISRM Suggested Methods*; International Society for Rock Mechanics, Pergamon Press: Oxford, UK, 1981.
41. Fairhurst, C.E.; Hudson, J.A. Draft ISRM suggested method for the complete stress-strain curve for intact rock in uniaxial compression. *Int. J. Rock Mech. Min. Sci.* **1999**, *36*, 279–289.
42. Wang, S.; Wang, L.G.; Tian, J.S.; Fan, H.; Jiang, C.Y.; Ding, K. An Experimental Study on the Effects of True Triaxial Loading and Unloading Stress Paths on the Mechanical Properties of Red Sandstone. *Minerals* **2022**, *12*, 204. [CrossRef]
43. Wang, S.; Wang, L.; Ren, B.; Ding, K.; Jiang, C.; Guo, J. Study of the mechanical characteristics of coal-serial sandstone after high temperature treatment under true triaxial loading. *Sci. Rep.* **2023**, *13*, 13036. [CrossRef]
44. Wang, X.; Liu, X.; Wang, E.; Li, X.; Zhang, X.; Zhang, C.; Kong, B. Experimental research of the AE responses and fracture evolution characteristics for sand-paraffin similar material. *Constr. Build. Mater.* **2017**, *132*, 446–456. [CrossRef]
45. Huang, X.; Bie, Z.; Wang, L.; Jin, Y.; Liu, X.; Su, G.; He, X. Finite element method of bond-based peridynamics and its ABAQUS implementation. *Eng. Fract. Mech.* **2019**, *206*, 408–426. [CrossRef]
46. Hibbitt; Sorensen, K. *ABAQUS: Theory Manual*; Hibbitt, Karlsson & Sorensen: Providence, RI, USA, 1997; Volume 2.
47. Tahmasebinia, F.; Yang, A.; Feghali, P.; Skrzypkowski, K. A Numerical Investigation to Calculate Ultimate Limit State Capacity of Cable Bolts Subjected to Impact Loading. *Appl. Sci.* **2023**, *13*, 15. [CrossRef]